JACS
JOURNAL OF THE AMERICAN CHEMICAL SOCIETY

Article

pubs.acs.org/JACS

Peptide Chain Dynamics in Light and Heavy Water: Zooming in on Internal Friction

Julius C. F. Schulz,[†] Lennart Schmidt,[†] Robert B. Best,[‡] Joachim Dzubiella,[§,∥] and Roland R. Netz*[,†]

[†]Fachbereich Physik, Freie Universität Berlin, 14195 Berlin, Germany

[‡]Department of Chemistry, University of Cambridge, Lensfield Road, Cambridge, CB2 1EW, United Kingdom

[§]Helmholtz-Zentrum Berlin für Materialien und Energie, 14109 Berlin, Germany

[∥]Institut für Physik, Humboldt-Universität zu Berlin, 12489 Berlin, Germany

Supporting Information

ABSTRACT: Frictional effects due to the chain itself, rather than the solvent, may have a significant effect on protein dynamics. Experimentally, such "internal friction" has been investigated by studying folding or binding kinetics at varying solvent viscosity; however, the molecular origin of these effects is hard to pinpoint. We consider the kinetics of disordered glycine-serine and α-helix forming alanine peptides and a coarse-grained protein folding model in explicit-solvent molecular dynamics simulations. By varying the solvent mass over more than two orders of magnitude, we alter only the solvent viscosity and not the folding free energy. Folding dynamics at the near-vanishing solvent viscosities accessible by this approach suggests that solvent and internal friction effects are intrinsically entangled. This finding is rationalized by calculation of the polymer end-to-end distance dynamics from a Rouse model that includes internal friction. An analysis of the friction profile along different reaction coordinates, extracted from the simulation data, demonstrates that internal as well as solvent friction varies substantially along the folding pathways and furthermore suggests a connection between friction and the formation of hydrogen bonds upon folding.

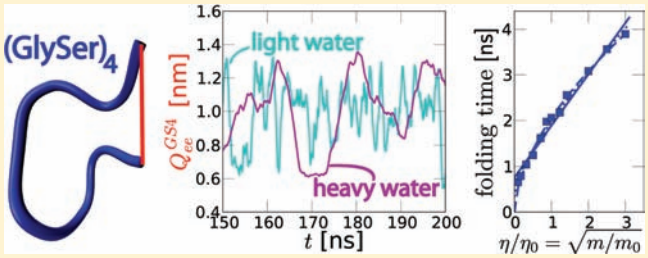

INTRODUCTION

It seems intuitively clear that the kinetics of protein folding and conformational transitions is not dictated by water viscosity alone but also by internal dissipation processes. In essence, if one could experimentally lower the viscosity of water without changing the folding free energy landscape, one would—for large enough proteins and in the hypothetical limit of vanishing solvent viscosity—still expect folding to be diffusive but with a diffusivity entirely determined by the internal friction of the protein. Apart from early stopped-flow studies on ribonuclease A,[1] the majority of experiments have demonstrated kinetic slowing down with increasing solvent viscosity: In a spectroscopic study on the folding of the α-subunit of tryptophan synthase, the folding rate was found to scale inversely with increased solvent viscosity, confirming that the rate-limiting step involves a solvent-dominated diffusional process, but the extrapolation to vanishing solvent viscosity resulted in a negligible folding time, therefore no indication of internal friction,[2] in agreement with more recent studies on protein L.[3] A study on the conformational relaxation following CO photodissociation in myoglobin on the other hand yielded a substantial viscosity-independent component upon extrapolation to vanishing solvent viscosity.[4] For various proteins that essentially fold downhill in the μs range close to the "speed limit", the existence of a nonzero internal friction was confirmed,[5−7] showing that folding over low barriers is particularly susceptible to internal friction effects;[8] internal friction has only been observed in one case for a larger protein.[9] Likewise, the loop formation dynamics of intrinsically disordered short peptides was found to be dramatically slowed down with added viscosifier.[10,11] In a particularly revealing study, the kinetics of α-helix and β-hairpin formation in two short model peptides was studied by laser temperature jumps and fluorescence detection:[12] The data were compared with two different laws for the folding time as a function of solvent viscosity: a pure power law predicting infinitely fast folding at vanishing solvent viscosity, and a linear law with a finite limiting folding time. Both forms essentially described the data equally well, partly reflecting the restricted available data range, since the aqueous solvent viscosity can experimentally not be lowered but only increased by the addition of viscogenic cosolutes. With the exception of very few protein studies,[7] the unwanted effects of viscogens on equilibrium properties cannot be excluded, which is particularly disturbing since denaturants (that are commonly added to counteract the stabilization due to viscogens) have also been shown to influence the peptide chain dynamics.[13]

Received: December 8, 2011
Published: March 13, 2012

   dx.doi.org/10.1021/ja211494h | J. Am. Chem. Soc. 2012, 134, 6273−6279

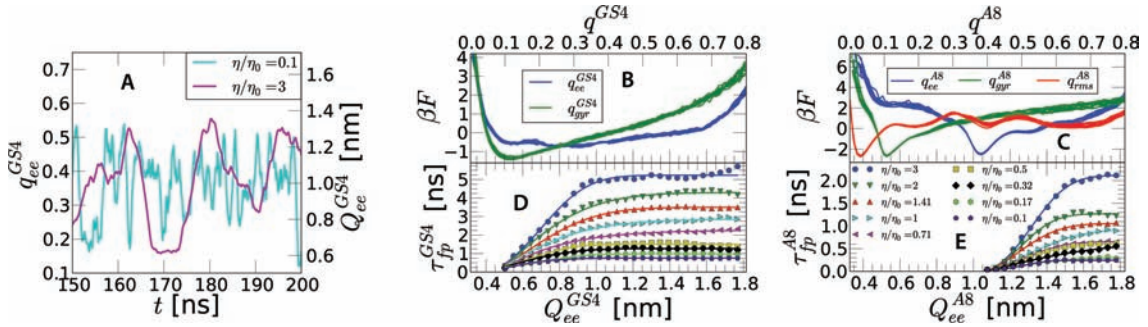

Figure 1. (A) Trajectories of the end-to-end distance Q_{ee}^{GS4} for $(GlySer)_4$ for the lowest and the highest water viscosities considered in our simulations, η/η_0 = 0.1 and 3. (B) Free energy $\beta F(Q)$ as a function of the end-to-end radius Q_{ee}^{GS4} (blue lines) and radius of gyration Q_{gyr}^{GS4} (green lines) for the unstructured peptide $(GlySer)_4$ for all different viscosities. (C) Free energy $\beta F(Q)$ for the helix-forming peptide Ala_8, here in addition results are plotted as a function of the rms deviation from the perfect helical state, q_{rms}^{Ala8} (red lines). (D) Mean first-passage times $\tau_{fp}^{GS4}(Q_{ee},Q_{ee}^{f})$ in terms of the end-to-end distance for final position Q_{ee}^{f} = 0.5 nm. (E) $\tau_{fp}^{A8}(Q_{ee},Q_{ee}^{f})$ for the final position Q_{ee}^{f} = 1.05 nm.

In an effort to assist and interpret these experimental efforts, Langevin simulations of protein folding in implicit solvent were performed.[14−16] As solvent friction is reduced, folding times decrease linearly with viscosity, as expected. But for viscosities orders of magnitude less than water, the functional dependence changes,[15] and eventually a turnover is observed, leading to a counterintuitive decrease of folding rate with decreasing viscosity.[14,16] This turnover is related to suppressed momentum dissipation into the Langevin heat bath at low friction[17] but presumably has no experimental relevance. Apart from this, the main drawback of standard implicit solvent simulations is that viscous damping, which mimics the solvent, acts in the same way on all residues, regardless of whether they face the solvent or are in the protein interior.[18] The decrease of the importance of solvent friction as one goes from disordered, solvent-rich conformations to compact structures is therefore not fully accounted for in such models. In explicit solvent simulations, on the other hand, mass rescaling provides a simple method for modifying the water viscosity: changing the water mass by a scaling factor c, the inertial force $\mathbf{F}$ following from Newton's equation of motion is invariant when simultaneously rescaling time by a factor $\sqrt{c}$,

$$cm\frac{d^2\mathbf{r}}{d(\sqrt{c}\,t)^2} = \mathbf{F} \tag{1}$$

meaning that at reduced water mass, all transport properties are accelerated, and in particular viscosity is reduced. By construction, equilibrium properties and therefore free energies are not influenced; consequently, this trick has previously been used to accelerate the equilibration of protein simulations in explicit solvent.[19,20] In the present paper we employ this procedure to study the viscosity-dependent kinetics of short peptides and a two-state protein, changing the solvent mass by more than two orders magnitude and in particular reaching the relevant regime of reduced solvent viscosities. Note that the modification of water mass in our simulation has no relation to the experimental distinction between normal and heavy water and is simply a trick to modify the viscosity of water. Since by changing the water mass all time scales are shifted, small solvent friction is accompanied by high heat conductivity, and therefore Kramer's turnover is not expected, suggesting that our simulation approach more closely captures the essence of experiments at modified solvent viscosity. Our simulations show clearly that internal friction effects exist. The separation into internal and solvent friction is nevertheless not straightforward, even when we locally resolve the friction profile along different reaction coordinates,[21,22] and although in simulations, we can substantially reduce the solvent viscosity.

Historically, the concept of internal friction arose for polymers in the context of dissipation due to the thermally activated crossing of dihedral barriers.[23] Shortly after, an alternative mechanism based on contacts between monomers that are not necessarily close neighbors along the backbone was suggested.[24] These contacts can be attractive (hydrogen bonds (HBs) are obvious candidates for this type) or steric and thus purely repulsive, giving rise to considerable kinetic slowing down in polymeric globules.[25] While local friction, e.g., due to dihedral barriers constitutes only a small correction to the long-time chain relaxation, it can be dominant at short times or for strongly stretched biopolymers.[26,27] Using a simple Rouse model that incorporates local internal friction, we show that the mean passage time for an incremental change of the end-to-end distance depends nontrivially on the solvent viscosity, exhibiting both linear as well as power-law behavior, depending on the relative strength of internal and solvent friction but always showing a nonzero folding time at vanishing solvent viscosity. The scaling form provided by the Rouse polymer model fits our simulation data quite well. Although protein kinetics is more complicated, involving also steric and HB effects, our Rouse model calculation is a first step toward understanding the complex entanglement of internal and solvent friction effects and rationalizes the occurrence of power laws for folding times as a function of solvent viscosity.

■ SIMULATION DETAILS

Our explicit water molecular dynamics simulations use the GROMACS[28] simulation package version 4.5, Amber ff03 force field,[29] and SPC/E water[30] model. In these simulations the presence of intrapeptide as well as peptide−water HBs is explicitly accounted for. The box size is 3.14 nm with 688 water molecules for Ala_8 and 3.18 nm with 711 water molecules for $(GlySer)_4$. Simulation times range up to 4 μs, pressure is set to 1 bar using a Parrinello−Rahman barostat,[31] and temperature to 300 K using a velocity rescaling thermostat.[32] The heat bath in our MD simulations couples to the average velocity in the simulation box[32] and therefore is expected to modify the dynamics only negligibly, in contrast to standard Langevin simulations. The different water masses used are between m/m_0 = 0.01 and 9, where m_0 denotes the standard water mass, and the integration time step has been adjusted accordingly. In

dx.doi.org/10.1021/ja211494h | J. Am. Chem. Soc. 2012, 134, 6273−6279

order to also treat larger proteins, we additionally perform simulations using a coarse-grained Go-type model for a 47-residue protein in explicit coarse-grained solvent (for further simulation details, see Supporting Information text).

RESULTS AND DISCUSSION

Simulations at Varying Water Mass. To study the effects of solvent viscosity on peptide dynamics, we consider two simple, eight amino acid peptides. The first, a $(GlySer)_4$ chain, is unstructured and has been widely studied experimentally,[10] the second is the helix forming peptide Ala_8; both peptide termini are capped. By changing the mass of water in the simulations, the water viscosity varies between $\eta/\eta_0 = (m/m_0)^{1/2} = 0.1$ and $\eta/\eta_0 = 3$. In Figure 1A we show the fluctuating end-to-end distance Q_{ee}^{GS4} (defined as the distance between the terminal amino acids) for $(GlySer)_4$ for the lowest and the highest viscosities, $\eta/\eta_0 = 0.1$ and 3, as a function of time, illustrating the clear difference in dynamics. In Figure 1B we show the free energy $\beta F(Q) = -\ln P(Q)$, which follows from the averaged probability distribution $P(Q)$, as a function of Q_{ee}^{GS4} (blue lines) and radius of gyration Q_{gyr}^{GS4} (green lines) for $(GlySer)_4$ for all different viscosities. Note that q variables denote rescaled versions of the original Q, mapping the domain between the smallest and the largest observed reaction coordinate (RC) values Q onto the interval $q = [0,1]$ and that $P(q)$ is normalized as $\int_0^1 dq P(q) = 1$. Figure 1C displays $\beta F(Q)$ for Ala_8, where in addition to q_{ee}^{Ala8} (blue lines), q_{gyr}^{Ala8} (green lines), we show F as a function of the root-mean-square (rms) deviation from the perfect helical state, q_{rms}^{Ala8} (red lines). We note that the free energy profiles for each RC and different water viscosities for both peptides agree closely with each other, thus matching our expectation that solvent viscosity does not influence equilibrium properties and in addition showing that our simulations are well equilibrated. The $(GlySer)_4$ free energy profiles are rather broad and reflect the lack of ordered structure, while the Ala_8 profiles exhibit pronounced minima corresponding to the folded α-helical state. A quantitative analysis of how solvent viscosity influences the peptide kinetics is possible by computing mean first-passage times $\tau_{fp}(Q,Q^f)$, which measure how long it takes, starting from a given position Q along the RC, to reach the final state Q^f for the first time. In Figure 1D we show $\tau_{fp}^{GS4}(Q_{ee},Q_{ee}^f)$ for the end-to-end distance for the final position $Q_{ee}^f = 0.5$ nm, and in Figure 1E we show $\tau_{fp}^{A8}(Q_{ee},Q_{ee}^f)$ for the final position $Q_{ee}^f = 1.05$ nm. The final positions are in both cases chosen as convenient (i.e., statistically prominent) product states in a prototypical folding reaction starting from $Q_{ee} > Q_{ee}^f$. As already suggested by the trajectories in (Figure 1A), the folding becomes slower with increasing viscosity and is fully confirmed by the results for the mean first-passage times for different water viscosities. A convenient and well-equilibrated measure for the folding speed is the Boltzmann-averaged mean first-passage time:

$$\overline{\tau}_{fp}(Q^f) = \int_{Q^f}^{\infty} dQ P(Q) \tau_{fp}(Q, Q^f) / \int_{Q^f}^{\infty} dQ P(Q) \quad (2)$$

If the solvent viscosity η were the only time scale in the folding kinetics, the ratio $\overline{\tau}_{fp}/(\eta/\eta_0)$ would be independent of η/η_0. The results in Figure 2A for the end-to-end distance of the $(GlySer)_4$ (blue) and Ala_8 peptides (red data points) exhibit a pronounced decrease of the rescaled folding time $\overline{\tau}_{fp}/(\eta/\eta_0)$ with η/η_0. Thus, the folding time $\overline{\tau}_{fp}$ decreases sublinearly with η/η_0 as $\eta/\eta_0 \to 0$, proving that finite internal friction exists both

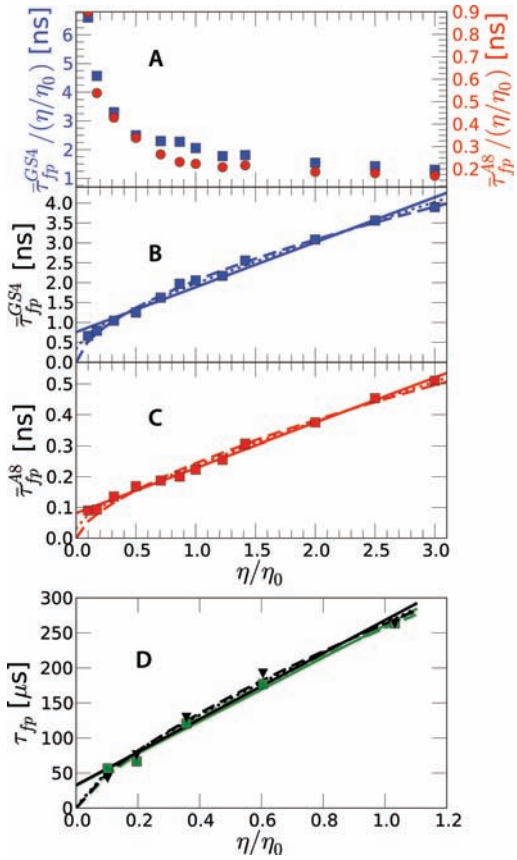

Figure 2. (A) Boltzmann-averaged mean first-passage time, eq 2, rescaled by the solvent viscosity, $\overline{\tau}_{fp}(Q^f)/(\eta/\eta_0)$, for the end-to-end distance of the $(GlySer)_4$ (blue) and Ala_8 peptides (red data points), as a function of η/η_0. The data clearly show that folding time is not proportional to η and therefore internal friction exists. (B) Averaged folding time $\overline{\tau}_{fp}$ for $(GlySer)_4$ as a function of the viscosity ratio η/η_0. (C) Analogous results for Ala_8. (D) Results for the averaged folding $\overline{\tau}_{fp}^f$ (green) and unfolding time $\overline{\tau}_{fp}^u$ (black) for the protein $1prb_{7-53}$ from a coarse-grained Go-type model. In B–D, fits according to eqs 3 (solid), 4 (broken), and 7 (dotted lines, $N = 10$ in B and C and $N = 47$ in D) are shown. Note that in D, eqs 4 and 7 are almost indistinguishable.

for the folding of $(GlySer)_4$ as well as Ala_8. Testing the relevance of the peptide dynamics to proteins is challenging because of the computational demands, even for the fastest-folding proteins. We therefore use instead a coarse-grained Go-type model[33] of the two-state 47 residue 3-helix bundle protein $1prb_{7-53}$[34] with explicit solvent (details in Supporting Information). Remarkably, we find a very similar nonlinear dependence of the folding and unfolding rates on viscosity, revealing a measurable internal friction even in this case. In Figure 2B–D we plot the averaged folding time $\overline{\tau}_{fp}$ for $(GlySer)_4$, Ala_8, and the coarse model for protein $1prb_{7-53}$ as a function of the viscosity ratio η/η_0 and compare it with two previously suggested heuristic fitting functions:[12]

$$\overline{\tau}_{fp} = \tau_{int} + \tau_{wat}\eta/\eta_0 \quad (3)$$

and

$$\overline{\tau}_{fp} = \tau_0(\eta/\eta_0)^{\alpha} \quad (4)$$

While both forms give fits of essentially equivalent quality, shown as solid and broken lines, only the linear form eq 3 allows a straightforward separation of the folding time into an

dx.doi.org/10.1021/ja211494h | J. Am. Chem. Soc. 2012, 134, 6273–6279

internal contribution τ_{int}, which would be the folding time in the hypothetical limit of vanishing solvent viscosity $\eta/\eta_0 \to 0$ and the water contribution τ_{wat}, which is the added folding time due to the presence of water. According to the linear model eq 3, the internal viscosity contribution makes up roughly half of the total folding time for the two peptides shown in Figure 2B,C, and for the protein in the coarse-grained model in Figure 2D, the internal contribution is much smaller (see Supporting Information for details). The power law form eq 4 allows no such separation into internal and solvent contributions to the folding time, rather introducing an exponent which turns out to be $\alpha = 0.59$ for $(GlySer)_4$, $\alpha = 0.73$ for $1prb_{7-53}$, and $\alpha = 0.66$ for Ala_8, quite close to experimental measurements for an α-helix forming peptide of $\alpha = 0.64$,[12] but at the same time leads to the nonintuitive extrapolation that folding occurs infinitely fast as solvent viscosity vanishes. We emphasize that both forms definitely assume that internal friction exists (otherwise we would have $\overline{\tau}_{fp} = \tau_0\eta/\eta_0$), but none is rigorously derived from a polymeric or protein model. This gap is filled by a Rouse-type calculation for the passage time of an ideal polymer chain with internal friction, results of which are shown as dotted lines in Figure 2B–D.

Passage Times from Rouse Model including Internal Friction. In the standard Rouse model for polymer dynamics, N connected beads at positions $\mathbf{R}_n$ with $n = 1, ..., N$ are subject to friction forces $-\xi_m d\mathbf{R}_n/dt$ that counteract bead motion proportional to the monomeric Stokes friction coefficient $\xi_m = 6\pi\eta a$, where a is the effective bead radius. The simplest mechanism for internal friction is bond friction that acts on the bond vector $\mathbf{R}_n - \mathbf{R}_{n-1}$ in the form of a force proportional to the bond stretching velocity, $-\xi_b d(\mathbf{R}_n - \mathbf{R}_{n-1})/dt$, where ξ_b is the bond friction coefficient that, to leading order, is independent of the solvent viscosity and only depends on dissipative processes within the polymer (e.g., due to dihedral barriers). Since each monomer participates in two bonds, the Langevin equation of motion takes in the continuum limit the symmetric form[24,27]

$$\xi_m d\mathbf{R}(n)/dt = (\kappa + \xi_b d/dt) d^2\mathbf{R}(n)/dn^2 + \mathbf{f}(n) \quad (5)$$

where $\kappa \sim k_B T/a^2$ is a spring constant ensuring an equilibrium bond length $\sim a$ and $\mathbf{f}(n)$ is a vectorial Gaussian random force. By normal-mode decomposition, eq 5 can be solved in closed form, and the final result for the autocorrelation function of the mean-squared end-to-end distance $C_{ee}(t) = \langle(\mathbf{R}_{ee}(t) - \mathbf{R}_{ee}(0))^2\rangle/\langle\mathbf{R}_{ee}^2\rangle$, with $\mathbf{R}_{ee} = \mathbf{R}(N) - \mathbf{R}(0)$, is[27] (see Supporting Information for full details of the calculation)

$$C_{ee}(t) = C_0 \sum_p^N (1 - e^{-t/\tau_p})/p^2 \quad (6)$$

Here C_0 is a normalization constant so that $C_{ee}(\infty) = 1$, the sum runs over odd mode numbers p only, and the mode relaxation time is $\tau_p = N^2\tau_m/p^2 + \tau_b$, where we have defined the monomer relaxation time $\tau_m = \xi_m/(\pi^2\kappa)$ and the bond relaxation time $\tau_b = \xi_b/\kappa$. For large times, $C_{ee}(t)$ approaches unity exponentially, $C_{ee}(t) \sim 1 - \exp(-t/(N^2\tau_m + \tau_b))$, where $N^2\tau_m$ is the polymeric or Rouse relaxation time. For intermediate times, in the so-called Rouse regime, $C_{ee}(t)$ grows as a power law, $C_{ee}(t) \sim (t/\tau_m)^{1/2}/N$. Most relevant for the present discussion based on the scenario of a protein diffusing in a 1D free energy landscape is the diffusive regime at short times, where we find three separate scaling ranges, depending on the relative strength of monomer and bond time scales: $C_{ee}(t) \sim t/\tau_b$ for dominating internal friction $N^2\tau_m < \tau_b$, $C_{ee}(t) \sim t/(N(\tau_b\tau_m)^{1/2})$ for intermediate internal friction $\tau_m < \tau_b < N^2\tau_m$, and $C_{ee}(t) \sim t/(N\tau_m)$ for negligible internal friction $\tau_b < \tau_m$ (see Supporting Information text). To connect to our simulation results for folding times, we define a mean passage time τ_{mp} by the condition that C_{ee} has reached a certain threshold value, $C_{ee}(\tau_{mp}) \equiv C_{ee}^*$, with C_{ee}^* chosen small enough so that one stays in the diffusive regime. A scaling function that contains all three regimes and accurately reproduces the numerical evaluation of eq 6 is $\tau_{mp}/C_{ee}^* = C_1\tau_b + C_2N(\tau_b\tau_m)^{1/2} + C_3N\tau_m$ (see Supporting Information text). The coefficients for $C_{ee}^* = 0.01$ and $N = 10$ are $C_1 = 1$, $C_2 = 0.9$, and $C_3 = 2.1$. Assuming a linear relation between τ_m and η as $\tau_m = \tau_m^0\eta/\eta_0$, where τ_m^0 is defined as the monomer relaxation time at reference solvent viscosity $\eta = \eta_0$, we obtain

$$\tau_{mp}/(C^*_{ee}\tau_b) = C_1 + C_2N\sqrt{\frac{\tau_m^0}{\tau_b}\frac{\eta}{\eta_0}} + C_3N\frac{\tau_m^0}{\tau_b}\frac{\eta}{\eta_0} \quad (7)$$

We note: (i) eq 7 contains two fitting parameters, an overall time scale, here, taken to be the bond relaxation time τ_b, and the ratio τ_m^0/τ_b between the monomer relaxation time at the reference solvent viscosity and the bond relaxation time, thus the number of fitting parameters is the same as in the previously discussed heuristic fitting forms eqs 3 and 4. (ii) Eq 7 combines key aspects of eqs 3 and 4, namely the folding time scale reaches a finite value for vanishing η, as in eq 3, and power-law behavior for intermediate times is obtained, as in eq 4. The resulting fits according to eq 7 in Figure 2B–D (dotted lines) are of the same quality as the other fits. (iii) For large chain lengths N, the first term in eq 7 that is independent of solvent viscosity becomes negligible; this is interesting in light of the experimental observation that internal friction is more pronounced for fast-folding (i.e., small) protein or protein domains,[5,6] with only one exception.[9]

The Rouse model discussed here is very simplified and neglects many effects and phenomena that are present and important in the actual peptide or protein dynamics. The main point of our Rouse model calculation is to demonstrate the complexity of chain kinetics when the solvent viscosity is varied, even for the relatively simple case of local internal friction (mimicking dihedral barrier effects) as defined by eq 5. While internal and solvent friction effects are additive for the relaxation time $\tau_p = N^2\tau_m/p^2 + \tau_b$ of each individual mode, as assumed in eq 3, the mode mixing that takes place when a kinetic observable such as the end-to-end radius is calculated, gives rise to power-law behavior, as assumed in eq 4. We now turn back to our more realistic friction scenarios based on simulations including interactions and HB effects.

Locally Resolved Friction Analysis. Some of the complexities observed in Figure 2B–D could have to do with the fact that a folding time integrates over the friction landscape, while the peptide moves from the starting configuration to the final configuration, particularly since the relative weight of internal friction should increase as one goes from open to more collapsed and hydrogen-bonded structures.[7] To look into this, we now resolve the friction profile locally. Assuming that a given RC evolves according to the Fokker–Planck equation:[35]

$$\frac{\partial}{\partial t}P(Q,t) = \frac{\partial}{\partial Q}\frac{1}{\beta\xi(Q)}e^{-\beta F(Q)}\frac{\partial}{\partial Q}P(Q,t)e^{\beta F(Q)} \quad (8)$$

dx.doi.org/10.1021/ja211494h | J. Am. Chem. Soc. 2012, 134, 6273–6279

where $P(Q,t)$ is the probability of having a configuration with RC value Q at time t and $\xi(Q)$ is the friction profile. Defining the round-trip time:

$$\tau_{rt}(Q, Q^f) = \text{sign}(Q - Q^f)[\tau_{fp}(Q, Q^f) + \tau_{fp}(Q^f, Q)] \quad (9)$$

as the time needed to start at Q, reach Q^f for the first time, start from Q_f again, and reach back to Q for the first time, one finds[22]

$$\tau_{rt}(Q, Q^f) = Z \int_{Q^f}^{Q} dQ' \beta\xi(Q') e^{\beta F(Q')} \quad (10)$$

where $Z = \int_{Q^{min}}^{Q^{max}} dQ e^{-\beta F(Q)}$ is the partition function which in our normalization is unity. The friction profile based on the round-trip time (see Supporting Information text) reads[22]

$$\beta\xi(Q) = \frac{\partial \tau_{rt}(Q, Q^f)/\partial Q}{Z e^{\beta F(Q)}} \quad (11)$$

which in Figure 3A is shown for different solvent viscosities for $(GlySer)_4$ in terms of the rescaled end-to-end distance

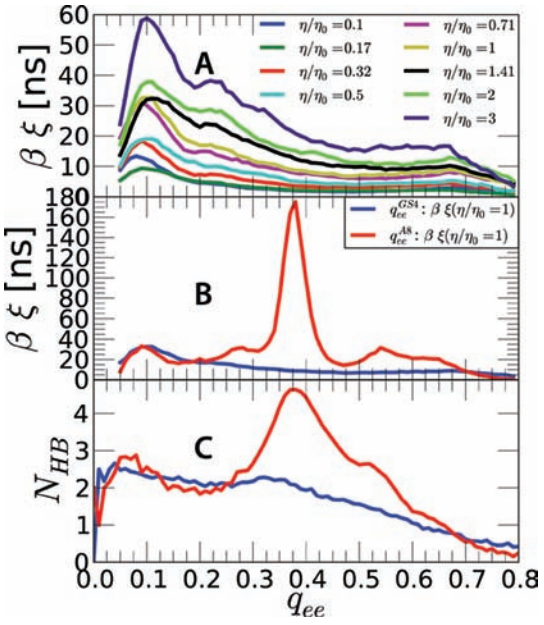

Figure 3. (A) Locally resolved friction profiles $\beta\xi(q_{ee})$ for different solvent viscosities for $(GlySer)_4$ as a function of the rescaled end-to-end distance q_{ee}. (B) $\beta\xi(q_{ee})$ at normal water viscosity $\eta/\eta_0 = 1$ for $(GlySer)_4$ (blue line) and Ala_8 (red line). (C) Number of intrapeptide HBs N_{HB} for $(GlySer)_4$ (blue line) and Ala_8 (red line).

coordinate q_{ee}. Indeed, the local friction increases with increasing η, and in addition, ξ goes up for smaller q_{ee}, i.e., when the peptide chain becomes more confined.[7] When comparing $\xi(q_{ee})$ at normal water viscosity $\eta/\eta_0 = 1$ for $(GlySer)_4$ (blue line) and Ala_8 (red line) in Figure 3B, we see that Ala_8 shows a friction maximum at an intermediate value of $q_{ee} \approx 0.4$. This can be compared with the number of intrapeptide HBs N_{HB} in Figure 3C. HBs are defined according to the distance–angle criterion that the acceptor–donor–hydrogen angle θ should be smaller than $\theta = 30°$ and the donor–acceptor distance smaller than 0.35 nm.[36] Indeed, the maximum in ξ at $q_{ee} \approx 0.4$ for Ala_8 roughly matches the maximum in N_{HB}, corresponding to the helical state; the naive expectation (which will be rectified below) would be that the total number of HBs determines local friction, meaning that the local friction should be high when the number of intrapeptide HBs is high.

In fact, the end-to-end distance is not the most natural RC to characterize friction in our two model peptides. Therefore in Figure 4 we show $\beta\xi$ as a function of the radius of gyration q_{gyr}

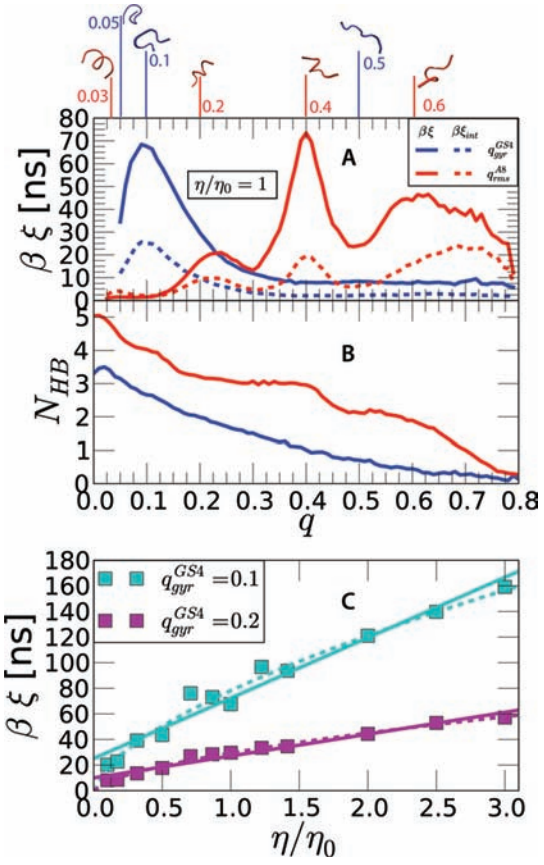

Figure 4. (A) Friction profiles $\beta\xi$ (solid lines) and internal contribution $\beta\xi_{int}$ (broken lines) at $\eta/\eta_0 = 1$ for $(GlySer)_4$ as a function of the rescaled radius of gyration q_{gyr} (blue) and for Ala_8 as a function of the rms from the perfect helical state q_{rms} (red). Representative simulation snapshots are shown at the top. (B) Corresponding number of intrapeptide hydrogen bonds. (C) $\beta\xi^{GS4}$ for $q_{gyr} = 0.1$ and $q_{gyr} = 0.2$ as a function η/η_0. Solid and broken lines denote linear and power-law fits according to eqs 3 and 4, respectively.

for $(GlySer)_4$ and as a function of the rms from the perfect helical state q_{rms} for Ala_8. For a disordered chain like $(GlySer)_4$, one would expect internal friction to be mainly due to unspecific intrapeptide HBs and to be increased in the collapsed state; indeed, ξ plotted versus q_{gyr} shows a pronounced maximum for small q_{gyr} in Figure 4A (blue solid line) that is paralleled by a maximum in N_{HB} in Figure 4B (blue line). Unexpectedly, for Ala_8, a pronounced maximum in ξ appears at $q_{rms} \approx 0.4$ (red solid line in Figure 4A) and thus shifted away from the fully folded state (around $q_{rms} \approx 0.1$), where N_{HB} has saturated to the maximum value. Scrutinizing N_{HB} for Ala_8 in Figure 4B (red line) more closely, one sees that the maximum in ξ^{A8} around $q_{rms} \approx 0.4$ correlates roughly with a sudden drop of N_{HB} around $q_{rms} \approx 0.45$. A possible connection between friction and variations in N_{HB} is suggested by the invariance of the Fokker–Planck equation (eq 8) under

dx.doi.org/10.1021/ja211494h | J. Am. Chem. Soc. 2012, 134, 6273–6279

coordinate rescaling according to $\tilde{Q} = \tilde{Q}(Q)$, if the functions Ψ, F, ξ are simultaneously rescaled as $\tilde{\Psi} = \Psi/\tilde{Q}'$, $\tilde{F} = F + \beta^{-1} \ln \tilde{Q}'$, $\tilde{\xi} = \xi/(\tilde{Q}')^2$, where $\tilde{Q}' \equiv d\tilde{Q}(Q)/dQ$. Thus an arbitrary friction profile $\tilde{\xi}(\tilde{Q})$ can be designed, including the limiting simple case of a constant friction $\tilde{\xi}(\tilde{Q}) = \tilde{\xi}_0$, while the kinetics stays invariant. Since all observables (and in particular the HB number N_{HB}) are not modified by the rescaling $\tilde{Q} = \tilde{Q}(Q)$, an explanation of $\xi(Q)$ in terms of equilibrium observables is spurious. Thus, the friction profile can only be linked to derivatives, such as $dN_{HB}(Q)/dQ$, which have similar transformation properties as $\xi(Q)$ itself. Indeed, when comparing ξ^{A8} in Figure 4A (red line) with N_{HB}^{A8} in Figure 4B (red line), we see that maxima in ξ^{A8} approximately correlate with regions where N_{HB}^{A8} changes pronouncedly with q_{rms}. A mechanistic interpretation of this would be that HB-related friction is particularly large when the number of HBs significantly changes along the RC, i.e., when additional HBs are created, most likely because formation of non-native HBs results in long-lived kinetic traps.[9] The importance of HBs for internal friction was clearly pointed out in previous work on the short-time kinetic energy partitioning in solvated carboxy-myoglobin.[37] That study also found salient differences in internal friction between various residue types, which is in line with the pronounced differences we find between the two peptides Ala_8 and $(GlySer)_4$, as clearly demonstrated in Figure 4A. It was suggested by the same authors that other interactions between side chains besides the formation of HBs are relevant for the magnitude and character of internal friction. This suggestion could in the future be studied by simulations similar to ours but for a wider collection of different residue types.

Finally, we check whether the local friction profile facilitates the separation into solvent and internal friction. To that end, in Figure 4C we plot the friction ξ^{GS4} for $q_{gyr} = 0.1$ and 0.2 as a function η/η_0. Similar to the averaged mean first passage times shown in Figure 2B, a linear fit as in eq 3 is possible (solid lines), but the data show clear signs of curvature, and a power-law fit according to eq 4 (broken lines) is equally accurate. Nevertheless, the broken lines in Figure 4A show the internal friction profiles $\xi_{int}(q)$ that are defined via the scaling form:

$$\xi(q) = \xi_{int}(q) + \xi_{wat}(q)\eta/\eta_0 \quad (12)$$

inspired by eq 3. $\xi_{int}(q)$ largely parallels the total friction profiles $\xi(q)$ (solid lines), but the intuitive expectation that ξ_{int} should dominate in the folded (HB-rich) state, while solvent friction, i.e., $\xi - \xi_{int}$, should dominate in the unfolded (open) state is not borne out by the data. This might have to do with the lack of a rigorous recipe for the division between solvent and internal friction (stressing again that the linear law in eq 12 is purely heuristic). Alternatively, the similar behavior of the internal friction profile $\xi_{int}(q)$ and the total friction profile $\xi(q)$ in Figure 4A could have a deeper origin and actually mean that water indirectly also influences HB-induced internal friction, possibly because whenever an intrapeptide HB breaks, a water molecule penetrates and serves as an intermittent HB donor or acceptor.

CONCLUSION

Our simulations clearly show that internal friction effects exist but at the same time demonstrate that the quantitative separation into internal and solvent friction is not straightforward. This is true even when we locally resolve the friction profile along different RCs,[21,22] and even though in simulations we can substantially reduce the solvent viscosity while making sure that free-energy folding profiles are not modified as viscosity changes. This has primarily to do with the lack of a simple but physically motivated definition of internal friction in terms of folding times or friction profiles. This complexity is corroborated by a simple Rouse-type model for the kinetics of a Gaussian polymer chain including internal local friction, for which the calculated passage times show power-law and linear behavior as a function of solvent viscosity, depending on the internal friction strength and the polymer size N. It is the polymeric, multiscale nature of the dynamics that gives rise to the power-law viscosity dependency of time scales in our model calculation and that turns out to be very similar to our simulations and to experimental observations of protein folding times.[12] In fact, an alternative explanation for power-law behavior based on the finite spatial range of spectroscopic probes has been previously given,[38] and in reality both mechanisms will be entangled.

ASSOCIATED CONTENT

Supporting Information

The derivation of the Rouse Model and detailed description of simulation protocols and analysis. This material is available free of charge via the Internet at http://pubs.acs.org.

AUTHOR INFORMATION

Corresponding Author

rnetz@physik.fu-berlin.de

Notes

The authors declare no competing financial interest.

ACKNOWLEDGMENTS

Financial support from the DFG via grants SFB 863 and NE810/8 is acknowledged. R.B. is supported by a Royal Society University Research Fellowship.

REFERENCES

(1) Tsong, T. Y.; Baldwin, R. L. *Biopolymers* **1978**, *17*, 1669−1678.
(2) Matthews, C. *Biochemistry* **1990**, *29*, 2149−2154.
(3) Plaxco, K.; Baker, D. *Proc. Natl. Acad. Sci. U.S.A.* **1998**, *95*, 13591−13596.
(4) Ansari, A.; Jones, C. M.; Henry, E. R.; Hofrichter, J.; Eaton, W. A. *Science* **1992**, *256*, 1796−1798.
(5) Qiu, L.; Hagen, S. J. *J. Am. Chem. Soc.* **2004**, *126*, 3398−3399.
(6) Pabit, S. A.; Roder, H.; Hagen, S. J. *Biochemistry* **2004**, *43*, 12532−12538.
(7) Cellmer, T.; Henry, E. R.; Hofrichter, J.; Eaton, W. A. *Proc. Natl. Acad. Sci. U.S.A.* **2008**, *105*, 18320−18325.
(8) Bryngelson, J. D.; Onuchic, J. N.; Socci, N. D.; Wolynes, P. G. *Protein* **1995**, *21*, 167−195.
(9) Wensley, B. G.; et al. *Nature* **2010**, *463*, 685−688.
(10) Bieri, O.; Wirz, J.; Hellrung, B.; Schutkowski, M.; Drewello, M.; Kiefhaber, T. *Proc. Natl. Acad. Sci. U.S.A.* **1999**, *96*, 9597−9601.
(11) Lapidus, L. J.; Steinbach, P. J.; Eaton, W. A.; Szabo, A.; Hofrichter, J. *J. Phys. Chem. B* **2002**, *106*, 11628−11640.
(12) Jas, G. S.; Eaton, W. A.; Hofrichter, J. *J. Phys. Chem. B* **2001**, *105*, 261−272.
(13) Nettels, D.; Gopich, I.; Hoffmann, A.; Schuler, B. *Proc. Natl. Acad. Sci. U.S.A.* **2007**, *104*, 2655−2660.
(14) Klimov, D. K.; Thirumalai, D. *Phys. Rev. Lett.* **1997**, *79*, 317−320.
(15) Zagrovic, B.; Pande, V. *J. Comput. Chem.* **2003**, *24*, 1432−1436.
(16) Best, R. B.; Hummer, G. *Phys. Rev. Lett.* **2006**, *96*, 228104.
(17) Kramers, H. A. *Physica* **1940**, *7*, 284−303.
(18) Pastor, R. W.; Karplus, M. *J. Phys. Chem.* **1988**, *92*, 2636−2641.

(19) Nguyen, P. H. *J. Chem. Phys.* **2010**, *132*, 144109.
(20) Lin, I.; Tuckerman, M. E. *J. Phys. Chem. B* **2010**, *114*, 15935−15940.
(21) Best, R. B.; Hummer, G. *Proc. Natl. Acad. Sci. U.S.A.* **2010**, *107*, 1088−1093.
(22) Hinczewski, M.; von Hansen, Y.; Dzubiella, J.; Netz, R. R. *J. Chem. Phys.* **2010**, *132*, 245103.
(23) Bazua, E. R.; Williams, M. C. *J. Chem. Phys.* **1973**, *59*, 2858.
(24) de Gennes, P. G. *J. Chem. Phys.* **1977**, *66*, 5825.
(25) Alexander-Katz, A.; Wada, H.; Netz, R. R. *Phys. Rev. Lett.* **2009**, *103*, 028102.
(26) Khatri, B. S.; Kawakami, M.; Byrne, K.; Smith, D. A.; McLeish, T. C. B. *Biophys. J.* **2007**, *92*, 1825−1835.
(27) Khatri, B. S.; McLeish, T. C. B. *Macromolecules* **2007**, *40*, 6770−6777.
(28) Hess, B.; Kutzner, C.; van der Spoel, D.; Lindahl, E. *J. Chem. Theory. Computation.* **2008**, *4*, 435−447.
(29) Duan, Y.; Wu, C.; Chowdhury, S.; Lee, M. C.; Xiong, G.; Zhang, W.; Yang, R.; Cieplak, P.; Luo, R.; Lee, T.; Caldwell, J.; Wang, J.; Kollman, P. *J. Comput. Chem.* **2003**, *24*, 1999−2012.
(30) Berendsen, H. J. C.; Grigera, J. R.; Straatsma, T. P. *J. Phys. Chem.* **1987**, *91*, 6269−6271.
(31) Parrinello, M.; Rahman, A. *J. Appl. Phys.* **1981**, *52*, 7182−7190.
(32) Bussi, G.; Donadio, D.; Parrinello, M. *J. Chem. Phys.* **2007**, *126*, 014101.
(33) Monticelli, L.; Kandasamy, S. K.; Periole, X.; Larson, R. G.; Tieleman, D. P.; Marrink, S. J. *J. Chem. Theor. Comp.* **2008**, *4*, 819−834.
(34) Wang, T.; Zhu, Y.; Gai, F. *J. Phys. Chem. B* **2004**, *108*, 3694−3697.
(35) Bryngelson, J. D.; Wolynes, P. G. *J. Phys. Chem.* **1989**, *93*, 6902−6915.
(36) Luzar, A.; Chandler, D. *Nature* **1996**, *379*, 55−57.
(37) Sagnella, D. E.; Straub, J. E.; Thirumalai, D. *J. Chem. Phys.* **2000**, *113*, 7702−7711.
(38) Cheng, R. R.; Uzawa, T.; Plaxco, K. W.; Makarov, D. E. *J. Phys. Chem. B* **2009**, *113*, 14026−14034.